

Actinic fluxes in broken cloud fields

A. Los, M. van Weele, and P. G. Duynkerke

Institute for Marine and Atmospheric Research Utrecht, Utrecht University, Utrecht, Netherlands

Abstract. Photochemical processes in the atmosphere are driven by solar ultraviolet radiation. The photodissociation rate coefficients of atmospheric species are determined by the actinic flux, which is defined as 4π times the mean ultraviolet intensity. Because of the presence of clouds the actinic flux can change drastically throughout the atmosphere. Therefore clouds have large effects on photodissociation rate coefficients. At cloud top, photodissociation rate coefficients can be 300% higher than in clear sky conditions. We use Monte Carlo simulations to investigate the reflectance, the transmittance, and the actinic flux for cloud fields at various degrees of cloudiness. Scattering processes in the clouds are due to cloud particles only. We do not take absorption of radiation into account. The atmosphere outside the clouds is assumed to be completely transparent. The simulated reflectance and transmittance of plane-parallel cloud fields and in broken cloud field conditions reproduce the results of previous model studies within statistical uncertainties. The results of actinic flux calculations for plane-parallel cloud fields agree with the results obtained with a doubling-adding algorithm. Horizontal and vertical actinic flux profiles in broken cloud fields are studied for various solar zenith angles and for different cloud optical thicknesses. The aim of the present model study is to obtain insight into the effect of broken cloud fields on the actinic flux.

1. Introduction

Photodissociation of atmospheric key molecules such as O_3 , NO_2 , CH_2O (formaldehyde), and H_2O_2 (hydrogen peroxide) by solar ultraviolet (UV) radiation plays an important role in the chemistry of the atmosphere. The photodissociation rate coefficient J of a photoactive molecule with an absorption cross section $\sigma(\lambda)$ and a photodissociation quantum yield $\phi(\lambda)$ is calculated by the integration of the product $\sigma(\lambda)\phi(\lambda)F(\lambda)$ over wavelength λ [Madronich, 1987]. Here $F(\lambda)$ is the actinic flux that quantifies the available dissociating radiation intensity. Both gas-phase chemistry and cloud chemistry are affected by varying actinic fluxes if clouds are present [e.g., Lelieveld and Crutzen, 1991]. Given the importance of photodissociation processes in atmospheric chemistry, the actinic flux needs to be studied in its various forms.

In the past the actinic flux in the atmosphere was studied in relation to several parameters including solar zenith angle and season, wavelength, surface pressure, height, and ground albedo [e.g., Demerjian *et al.*, 1980; Finlayson-Pitts and Pitts, 1986]. The effect of atmospheric constituents on the actinic flux was also studied before. Gaseous absorption by ozone, extinction by particulate matter, and especially scattering by cloud drops were recognized as important physical processes that influence the actinic flux [Madronich, 1987; Tsay and Stamnes, 1992; van Weele and Duynkerke, 1993; Ruggaber *et al.*, 1994]. Measurement studies showed that clouds make a large impact on the actinic flux [Junkermann, 1994; Vilà-Guerau de Arellano *et al.*, 1994; van Weele *et al.*, 1995].

The studies that considered cloud effects concluded that cloud optical thickness τ , which determines cloud albedo, is the most important optical property of a cloud. However, two other optical parameters are needed for a complete descrip-

tion of the radiative effect of a cloud: the scattering phase function, generally denoted by an asymmetry parameter g , and the single scattering albedo ω . These optical parameters can be related to cloud microphysical characteristics. The liquid water content and the effective radius and effective variance of the drop size distribution are the relevant microphysical parameters for radiative transfer in clouds [Hansen and Travis, 1974; van Weele and Duynkerke, 1993; Damiano and Chylek, 1994].

The aforementioned studies of the effect of clouds on the actinic flux considered stratiform clouds only (e.g., stratus or nimbostratus). Obviously, many clouds have intermittent structure. Broken clouds with cellular patterns are typically composed by cumulus or stratocumulus [Nicholls and Leighton, 1986]. However, numerous studies on radiative transfer show that radiative transfer through broken cloud fields differs considerably from radiative transfer through plane-parallel clouds. The objective of the present study is therefore to examine the effect of broken cloud fields on the actinic flux. Although several authors have recognized that the effect of broken cloud fields on the actinic flux is an important topic for further study, to our knowledge no results of studies of this kind have yet been published. We hope that this study will increase our knowledge about photochemical processes in the troposphere and particularly about the radiative effect of clouds on photochemistry.

In this study we simulate radiative transfer in broken cloud fields by a Monte Carlo model. Photons are tracked as they pass through the cloud field. The photon path in the cloud field is determined by the free path length and by the phase function. We simulate the reflectance, the transmittance, and actinic fluxes for both plane-parallel and broken cloud fields at various degrees of cloudiness. Where possible, the results are compared with results of previous model studies. In the case of plane-parallel clouds we compare our calculations with accurate one-dimensional calculations (doubling-adding algorithm [de Haan *et al.*, 1987; van de Hulst, 1980]). Our results for the

Copyright 1997 by the American Geophysical Union.

Paper number 96JD03123.
10.1029/96JD-03123\$09.00

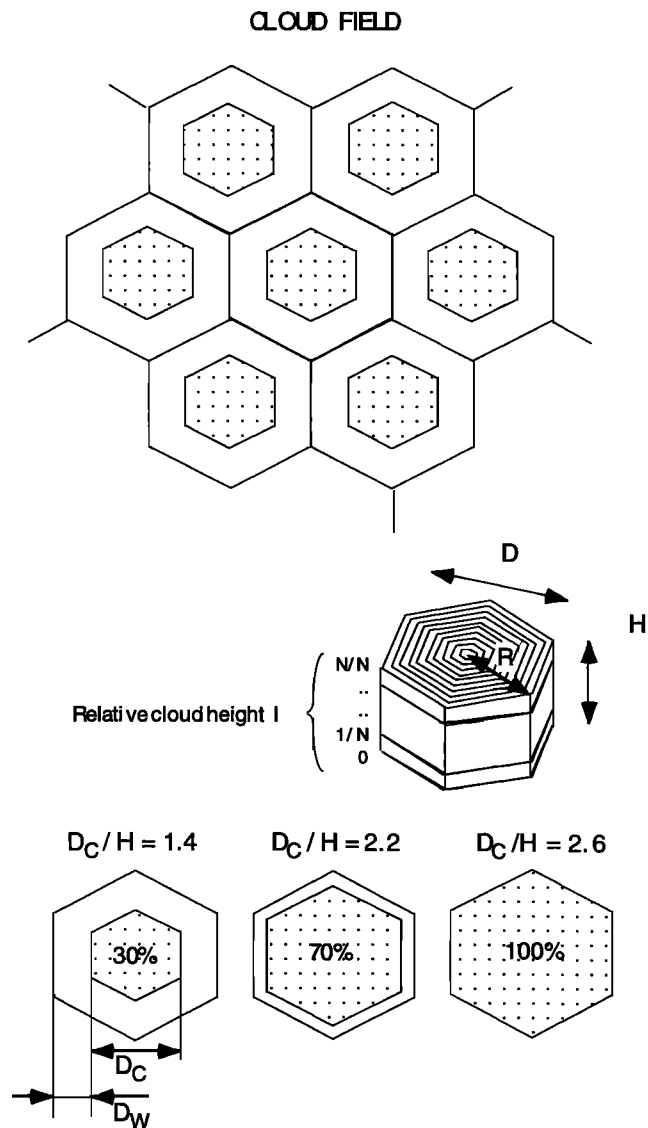


Figure 1. Geometry of the cloud field. A hexagonal cell consists of a core region (cloud cell) of hexagonal shape with “diameter” D_C and a wall region (cloud gap) of width D_W . The hexagonal cell is subdivided in 275 parts consisting of $N = 11$ vertically equidistant in-cloud surfaces (referred to as relative cloud heights) and 25 horizontally concentric hexagonal rings of equal area. The aspect ratio is equal to D_C/H , where H is the cloud height. The cloud cover c is 30%, 70%, and 100%. Cloud top and cloud base are flat surfaces. We use periodic boundary conditions; that is, the cloud field is stretched over a horizontally infinite domain.

reflectance and the transmittance in broken cloud fields are compared with the results reported by Bréon [1992]. He investigated the angular distribution patterns of radiance exiting from a cloud layer at various degrees of cloudiness and for different cloud optical properties and solar zenith angles. The patterns vary according to the cloud geometry, optical thickness, cloudiness, and solar zenith angle. Some differences between our calculations and those of Bréon arise because Bréon used a regular grid of cylindrical clouds, whereas we use a regular grid of hexagonal clouds. Moreover, Bréon used 10^5 photons in his Monte Carlo simulations, whereas in our study we used 5×10^5 photons.

Section 2 outlines the geometry and the radiative fluxes of the cloud fields. We explain how actinic fluxes can be evaluated from Monte Carlo simulations and how the actinic flux relates to the reflectance and transmittance of the cloud layer. In section 3 we present statistical properties and results of the Monte Carlo model. Horizontal and vertical profiles of the actinic flux are shown at various degrees of cloudiness and are shown for different solar zenith angles and cloud optical thicknesses. In section 4 we present some of our conclusions.

2. Monte Carlo Simulation

Because of increasing computer power, Monte Carlo simulations have become very accurate and are particularly worthwhile when standard plane-parallel theory of radiative transfer cannot be applied. Currently, three-dimensional radiative transfer methods are also being developed, both in analytical terms [Stephens, 1988; Kobayashi, 1991; Li et al., 1994a] and in more pragmatic approaches [Filyushkin and Lilly, 1993]. Here we give preference to Monte Carlo simulations because of their conceptual simplicity and flexibility.

Monte Carlo simulation studies are concerned primarily with the reflectance of cloud fields and the development of parametrizations for general circulation models [e.g., Welch and Wielicki, 1984; Bréon, 1992; Jonas, 1994; Li et al., 1994b]. Further, Monte Carlo simulations are used to retrieve cloud parameters from satellite observations, including cloud albedo, cloud optical thickness, type of scatterers (water drops versus ice crystals), and cloud structure [e.g., Coakley, 1991; Jonas, 1992; Kobayashi, 1993; Takano and Liou, 1995].

In this study the Monte Carlo simulation method is used to investigate the effect of broken cloud fields on radiative fluxes, that is, on cloud reflectance, on cloud transmittance, and on actinic flux, under various cloud conditions.

2.1. Model Description

The model described here was originally developed by Jonas [1992]. The main differences between the program developed by Jonas and our present program are the added actinic flux evaluation routines.

The broken cloud fields which are composed of cumulus or stratocumulus can be approximated by cylinders of hexagonal shape [Jonas, 1992]. Therefore the clouds of the present Monte Carlo model are implemented with a hexagonal geometry (Figure 1). Furthermore, the hexagonal structure is simple enough to keep the labor for geometric calculations within reasonable proportions. The incoming radiation originates from a photon point source under zenith angle θ_0 and azimuth angle ϕ_0 and illuminates the broken cloud field randomly, mutual shadowing being taken into account.

A single hexagonal cell consists of a core region (cloud cell) of hexagonal shape with “diameter” D_C and a wall region (cloud gap) of width D_W . This setup permits us to make a distinction between the cloud optical properties of the core region and the surrounding wall region. In order to allow the representation of horizontal and vertical profiles of actinic flux, the clouds are divided into azimuth-independent parts. Therefore each hexagonal cell consists of 11 vertically equidistant in-cloud surfaces, top and bottom surface included (Figure 1). The in-cloud surface is referred to as relative cloud height I ($I = 0, 1/N, \dots, N/N; N = 11$). On each surface, 25 horizontally concentric hexagonal rings of equal area are distinguished. With this subdivision of the cloud cell into $11 \times$

25 = 275 cloud parts, detailed calculations of cloud radiative fluxes are possible, and horizontal and vertical flux profiles can be obtained. The aspect ratio is equal to the diameter of the core region divided by the cloud height D_c/H . In this study, geometrical cloud height is fixed at $H = 400$ m. Therefore the aspect ratio varies with cloud cover (Figure 1). Cloud cover c is defined as the ratio of the core region area to the area of the hexagonal cell. The “radius” R of a hexagonal cell is equal to 600 m. Cloud top and cloud base are flat surfaces. The cloud field is stretched over a horizontally infinite domain.

Except for the clouds the atmosphere is assumed to be completely transparent; that is, the model takes no account of the interaction of radiation with the atmosphere outside the clouds. Although several physical processes affect the solar UV radiation intensity (e.g., molecular scattering, absorption by ozone, and scattering by aerosol particles), we consider scattering processes by cloud drops only. Because we are interested mainly in UV radiation, we also ignore absorption by cloud drops (single scattering albedo $\omega = 1$). Previous studies have suggested that the large-scale geometric effects outweigh microphysical structure effects [Coakley, 1991; Barker, 1994]. Therefore the clouds are assumed to be internally homogeneous; that is, possible variations in liquid water content and drop size distribution are ignored.

Applied to the radiative transfer in clouds, the Monte Carlo method numerically simulates the tracks of a large number of photons in a cloud field as they interact with cloud particles, that is, water droplets. Random processes determine the mean free path length between two interactions and the scattering angle according to the scattering phase function. Both the angular distribution of the scattered radiation and the mean free path length depend on cloud microphysical characteristics.

The mean free path length s is expressed as

$$s = -\ln(1 - \text{RAN})/\beta_e \quad (1)$$

where RAN is a random number with $0 \leq \text{RAN} < 1$. The extinction coefficient β_e is given by the integration of the product of the extinction cross section $\sigma_e(r)$ and the size distribution function $n(r)$ over cloud particle size r . However, because the radius of cloud drops is typically much larger than UV wavelengths, we can approximate β_e by using the effective radius r_{eff} of the size distribution, which yields

$$\beta_e = 2\pi r_{\text{eff}}^2 N_d \quad (2)$$

where N_d is the number density of the cloud drops. The cloud optical thickness (or cloud optical depth) τ is a macrophysical cloud parameter that combines the extinction coefficient β_e with the cloud dimension. We obtain τ by integration of β_e over the geometric height of the cloud. Since we only consider homogeneous clouds, τ becomes the product of β_e and cloud height H ($H = 400$ m). In our simulations we used $\tau = 6$ for optically thin clouds and $\tau = 20$ and 50 for optically thick clouds. Assuming an effective radius of $r_{\text{eff}} = 10 \mu\text{m}$, an optical thickness of $\tau = 20$ therefore corresponds to a number density N_d of 80 cm^{-3} .

It is possible to express the phase function in various ways, depending on the type of cloud particles considered. For the calculation of radiative fluxes in the atmosphere an analytical expression for the phase function in terms of an asymmetry factor g has been proposed; it is referred to as the Henyey-Greenstein phase function [Pomraning, 1988].

The Henyey-Greenstein phase function is used in the

present study. The main advantage of using this phase function is that the corresponding normalized cumulative scattering phase function $\tilde{P}_{\text{H-G}}$ can be expressed analytically in the following form:

$$\tilde{P}_{\text{H-G}}(\cos \theta_s) = \frac{1-g^2}{2g} \left[\frac{1}{1-g} - \frac{1}{(1+g^2-2g \cos \theta_s)^{1/2}} \right] \quad (3)$$

This function, with $0 \leq \tilde{P}_{\text{H-G}} \leq 1$, is synonymous with the probability density function for the angle of the scattering processes. The scattering angle θ_s is defined as the angle between the direction of propagation of the photon before and after the scattering event. The scattering angle is thus obtained by a random process according to the cumulative Henyey-Greenstein phase function. Resolving the cumulative scattering phase function $\tilde{P}_{\text{H-G}}$ for θ_s , one obtains

$$\theta_s = \cos^{-1} \left\{ \frac{1}{2g} \left[1 + g^2 - \left(\frac{1-g^2}{1+g-2g \text{RAN}} \right)^2 \right] \right\} \quad (4)$$

where RAN is a random number (with $0 \leq \text{RAN} < 1$) replacing $\tilde{P}_{\text{H-G}}(\cos \theta_s)$.

In our Monte Carlo simulations we used an asymmetry factor $g = 0.85$. The results of the doubling-adding algorithm, which are used for comparison purposes in the present study, are obtained with the same phase function and the same asymmetry factor.

In some studies, Mie phase functions are used. Then, the size distribution (effective radius) of the particles as well as their complex refractive index are important parameters. For comparisons with the results presented by Bréon [1992] we also used his Mie phase function for a cumulus cloud type droplet distribution. However, because no analytical expression for this Mie function is available, the scattering angle is obtained by interpolation of the cumulative Mie phase function that was calculated at 101 intervals between 0 and 1. This interpolation procedure introduces an extra approximation in the evaluation of the scattering angles which is not required when the Henyey-Greenstein phase function is used [Jonas, 1994].

2.2. Derivation of Radiative Quantities From a Monte Carlo Model

In the Monte Carlo model the incoming photons, which are randomly distributed, illuminate the cloud field at zenith angle θ_0 . In the clouds the photons are redistributed by multiple scattering processes that depend on the cloud optical properties and are finally emitted above or below the cloud field (no absorption). When only photons are counted, information about the radiation field itself is still not complete. Here we explain how various radiative quantities can be derived from photon counts.

A radiative flux is defined as the angular integrated radiance incident on a surface (units of W m^{-2}). Simulated radiative fluxes are therefore determined by counting the number of photons that pass through horizontal surfaces. However, if the directions of the photons passing through such a surface are known, then the radiance $I(\tau, \theta, \phi)$ can be described as the flux of energy transported in a given direction across a unit area perpendicular to the direction of propagation (units of $\text{W m}^{-2} \text{sr}^{-1}$).

The irradiance $E(\tau)$ is defined as the flux of energy incident from one hemisphere which is transported across a surface of unit area (units of W m^{-2}). The irradiance is therefore simulated by counting the number of incident photons per unit

area. Photons that are incident from directions normal to the surface are more likely to pass through that surface than photons that are incident from slant directions. This probability decreases with decreasing μ , where μ is the cosine of the angle between the direction of incidence of the photons and the normal of the surface.

For a molecule that is positioned on a surface the probability of being hit by a photon is equal for all incident directions of the photons. The actinic flux $F(\tau)$, that is, the number of photons passing through a surface per unit area irrespective of the direction of incidence, is therefore derived by counting the photons passing through the surface both upward and downward and weighting them with a factor μ^{-1} (where μ is again the cosine of the angle between the direction of incidence of the photons and the normal to the surface).

The albedo is calculated as the ratio of the number of upward escaping photons to the number of incoming photons. The angular distribution of the reflected radiation, or reflectance, is obtained by counting the number of upward emitted photons in zenith and azimuth angle intervals of the hemisphere above the cloud field. The angular distribution of the radiation escaping from the cloud can be written in terms of a bidirectional reflectance distribution function (BRDF) or a bidirectional transmittance distribution function (BTDF) for the reflected and transmitted radiation, respectively. The BRDF is defined as the ratio of the reflected radiance distribution to that of an isotropic surface reflecting the same irradiance. The BTDF is defined in the same way as the BRDF but for the transmitted radiation. By azimuthally averaging the angular distribution of the radiation, one obtains an azimuth-averaged reflectance distribution function (ARF) or an azimuth-averaged transmittance distribution function (ATF). The ARF(μ) is defined as the ratio of the azimuth-averaged reflected radiance distribution to that of an isotropic surface reflecting the same irradiance

$$\text{ARF}(\mu) = \frac{I \uparrow (0, \mu)}{[E \uparrow (0)/\pi]}. \quad (5)$$

The ARF(μ) is normalized according to

$$\int_0^1 \text{ARF}(\mu) 2\mu d\mu = 1. \quad (6)$$

Here $E \uparrow (0)$ is the upward irradiance and $I \uparrow (0, \mu)$ is the azimuth-averaged radiance for $\tau = 0$. The ATF is defined in the same way as the ARF but for the transmitted radiation.

The albedo A is defined as

$$A(\mu_0) = \frac{E \uparrow (0)}{E_0} = \frac{E \uparrow (0)}{\mu_0} \quad (7)$$

with $\mu_0 = \cos \theta_0$ and $E_0 = \mu_0 F_0$. The incident irradiance is denoted by E_0 , and the incident actinic flux $F_0 = 1$.

In this paper we use the term actinic flux enhancement $C_F(\tau)$, which is defined as the ratio of the actual actinic flux to the actinic flux of a completely transparent atmosphere; that is, $F_0 = 1$. Given the ARF(μ), the actinic flux enhancement at cloud top $C_F(\tau = 0)$ can be calculated according to

$$C_F(0) = \frac{F_0 + F \uparrow (0)}{F_0} = 1 + 2\pi \int_0^1 I \uparrow (0, \mu) d\mu. \quad (8)$$

Using (5) and (7), we find

$$C_F(0) = 1 + 2\mu_0 A(\mu_0) \int_0^1 \text{ARF}(\mu) d\mu. \quad (9)$$

The actinic flux enhancement at cloud base, $C_F(\tau = \tau_c)$, is described in the same way as for $C_F(\tau = 0)$, but for the transmitted radiation T and the azimuth-averaged transmittance distribution function ATF,

$$C_F(\tau_c) = 2\mu_0 T(\mu_0) \int_0^1 \text{ATF}(\mu) d\mu. \quad (10)$$

The actinic flux enhancement at cloud top, $C_F(\tau = 0)$, and cloud base, $C_F(\tau = \tau_c)$, can be derived in two different ways. The actinic flux enhancement given by (9) and (10) is obtained from the cosine of the solar zenith angle μ_0 , the albedo, and the ARF (through (9)), and from μ_0 , the transmittance, and the ATF (through (10)). By direct estimation the counted photons passing through the 275 parts of the subdivided cloud are weighted by their factor μ^{-1} which yields the actinic flux enhancement profiles for the entire cloud field. The advantage of using (9) is that the ARF has been presented by several other authors before. Application of (9) to ARFs and to albedos of other studies yields directly the actinic flux enhancement in relation to the geometry and assumptions made in those studies.

3. Results

3.1. Reflectance and Transmittance

Monte Carlo simulation results for the albedo, the BRDF/BTDF, and the ARF/ATF are presented. We compare results for (1) plane-parallel clouds with the results of the doubling-adding algorithm and (2) broken cloud fields at varying degrees of cloudiness with the results of earlier Monte Carlo studies such as those by Bréon [1992].

The doubling-adding algorithm contains an accurate radiative transfer calculation method [de Haan *et al.*, 1987; Stammes, 1993]. For plane-parallel clouds the results of the doubling-adding algorithm yield the same radiance distribution functions and actinic flux enhancement factors at cloud top and bottom as those produced by the Monte Carlo model of the present study. For both models the Henyey-Greenstein (H-G) phase function with an asymmetry factor g of 0.85 is used.

To limit the scope of this study, we analyze cloud radiative quantities with only one phase function. Therefore we present results with the H-G phase function only, except in the case of simulations of cloud reflectivities, which are also presented with the Mie phase function used by Bréon [1992].

The statistical properties of the Monte Carlo simulation method are considered. Figure 2 shows the relative standard errors of the albedo, the ARF, the actinic flux enhancement, and the BRDF for the Sun at zenith ($\theta_0 = 0^\circ$). The values marked with symbols in Figure 2 correspond to the maxima of the relative standard errors of the Monte Carlo simulations.

The photons that are escaping from the cloud field are binomially distributed. The log-log plot of Figure 2 shows that the simulations are proportional to the binomial $1/\sqrt{N}$ law. Consequently, increasing the number of photons by 1 order of magnitude will decrease the relative standard error by a factor of $\sqrt{10}$.

The highest relative standard errors are found for the BRDF (as in the case of the BTDF) because of small photon counting intervals (viewing zenith angle intervals) which cause low photon count rates. Consequently, the curve for the BRDF is not linear. In order to keep the relative standard errors lower than about 10% for all distribution functions we used 5×10^5 photons per simulation.

The difference in the relative standard error σ_r in two Monte Carlo simulations that use different number of photons is given by

$$\sigma_r(n) - \sigma_r(m) = \frac{\sqrt{m} - \sqrt{n}}{\sqrt{mn}} \sqrt{\frac{1-p}{p}}$$

where m and n are numbers of photons ($m > n$) and p is the probability that the radiation will scatter in one of the viewing zenith angle intervals.

3.1.1. Plane-parallel clouds. An important optical cloud characteristic is the albedo of the plane-parallel cloud field. Table 1 contains the albedo obtained with the Monte Carlo simulation of *Bréon* [1992], the doubling-adding algorithm, the present model study for cloud optical depths τ of 6, 20, and 50, and solar zenith angles θ_0 of 0° and 60° .

The model studies with the H-G phase function yield similar albedos. The model of *Bréon* [1992] was run with 1×10^5 photons and the present model study with 5×10^5 , which explains the discrepancies between the results of the two Monte Carlo simulations and the Mie phase function.

The radiation field of the plane-parallel cloud is represented by the bidirectional reflectance distribution function (BRDF) and by the bidirectional transmittance distribution function (BTDF). Figure 3a shows the BRDF of the Monte Carlo simulation for $\tau = 50$ and $\theta_0 = 60^\circ$. The corresponding BRDF obtained with the doubling-adding algorithm is presented in Figure 3b, which shows good agreement with the present Monte Carlo simulation. To compare the doubling-adding algorithm (DAA) with the Monte Carlo (MC) simulation, the ratio (MC-DAA)/DAA is calculated and depicted in Figure 3c. The discrepancy between the Monte Carlo simulation and the doubling-adding algorithm is about 20% at the viewing azimuth angle interval $63^\circ < \phi \leq 81^\circ$ and for $0.0 < \mu \leq 0.1$ (i.e.,

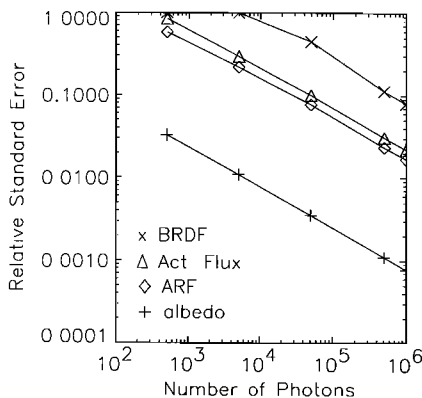


Figure 2. Log-log plot of the relative standard error of the albedo, the azimuth-averaged reflectance distribution function (ARF), the actinic flux enhancement, and the bidirectional reflectance distribution function (BRDF) versus the number of photons used in the Monte Carlo simulation. The curves show that the simulations are proportional to the binomial $1/\sqrt{N}$ law. The simulations are obtained for $\tau = 20$ and $\theta_0 = 0^\circ$.

Table 1. Albedo as Reported by *Bréon* [1992] and From Our Study Obtained With the Doubling-Adding Algorithm, and the Monte Carlo Simulation

θ_0	τ	Bréon (Mie), %	This Study		Doubling-Adding (H-G), %
			Mie, %	H-G, %	
0°	6	na	na	28.1	28.2
	20	61	60.5	61.7	61.7
	50	81	80.3	81.0	81.0
60°	6	na	na	49.9	49.9
	20	73	73.3	73.8	73.8
	50	87	86.7	87.1	87.0

The results are given for overcast conditions. H-G, Henyey-Greenstein.

viewing zenith angle interval $84^\circ \leq \theta < 90^\circ$). For all other viewing angle intervals the deviations are lower than the statistical uncertainties.

Figure 4 shows the BRDF obtained with the present Monte

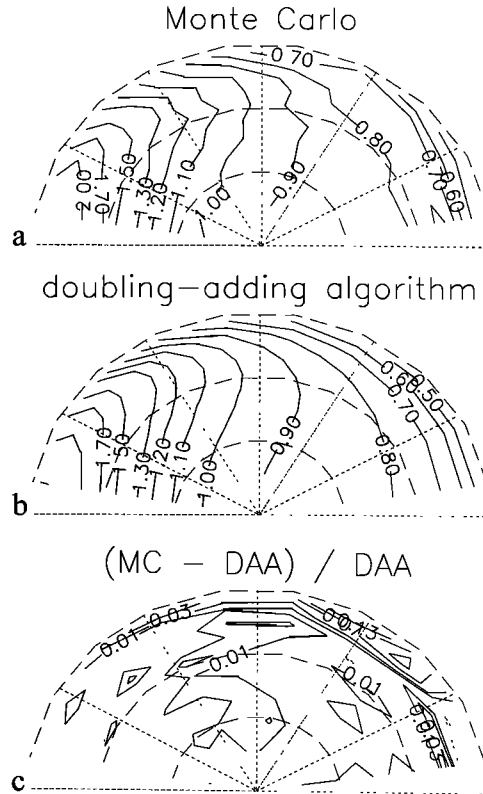


Figure 3. BRDF for overcast conditions obtained with (a) the Monte Carlo simulation for $\tau = 50$ and $\theta_0 = 60^\circ$ and with (b) the doubling-adding algorithm (DAA) for the same parameters as with the Monte Carlo (MC) simulation. The radius of Figures 3a and 3b is a linear function of the viewing zenith angle θ (with $0^\circ \leq \theta < 90^\circ$) and the polar angle is the viewing azimuth angle ϕ (Sun is at 0° , on the right-hand side) in increments of 30° . The contour intervals are 0.1 between 0.0 and 1.3, and the other contour levels are 1.5, 1.7, 2.0, 2.5, and 3.0. (c) The discrepancies between the BRDFs. The contour levels in Figure 3c are equal to the relative error which is described by the ratio (MC-DAA)/DAA. The radius and the polar angle are the same as in Figures 3a and 3b. The contour levels are -0.05 (dotted line), 0.01, 0.03, 0.07, and 0.13.

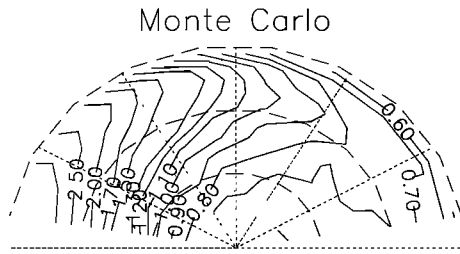


Figure 4. Same as Figure 3a, but for $\tau = 6$.

Carlo model for a thinner, plane-parallel cloud with $\tau = 6$. The solar zenith angle $\theta_0 = 60^\circ$. The optically thin cloud field produces a strongly forward directed radiation field. For optically thick cloud fields with $\tau = 50$ (Figure 3a), the number of interaction processes is more than 10 times higher than a cloud field with $\tau = 6$. Consequently, the radiation in clouds with $\tau = 50$ is highly diffusive, producing a radiation field above the plane-parallel cloud which reduces the information about the incoming radiation field.

The BRDF contains very detailed information about the cloud reflectance, for example, the maximum in the forward direction and the general decrease toward the limb. These cloud reflectance characteristics are more evident when one looks at the azimuth-averaged reflectance distribution function ARF. Figures 5a and 6a present the ARF obtained with the Monte Carlo simulation for a plane-parallel cloud field at varying solar zenith angles θ_0 and for $\tau = 20$ and 6, respectively. The general decrease in the ARF toward the limb is due to the fact that the in-cloud radiation passing parallel to the cloud top surface is less likely to escape than the cloud top radiation directed perpendicularly to the cloud top surface. This phenomenon known as the limb-darkening effect is also found at cloud bottom and can be seen in Figure 5b, which shows the corresponding ATF of the ARF in Figure 5a for $\tau = 20$. The incoming radiation from different solar zenith angles θ_0 has no effect on the ATF; that is, the transmitted radiation is completely diffuse. Figure 6b shows the ATF for $\tau = 6$, corresponding to the ARF in Figure 6a. The low cloud optical thickness lets one distinguish the transmitted radiation at cloud bottom as a function of the solar zenith angle θ_0 ; that is, the direction of the incident radiation can be more easily detected than in the case of the cloud field with $\tau = 20$.

The ARF of the doubling-adding algorithm is calculated for overcast conditions with $\tau = 50$ at a solar zenith angle $\theta_0 = 60^\circ$. The difference between the ARF of the doubling-adding algorithm and the present Monte Carlo simulation reaches a maximum of 2.6% at the limb (i.e., viewing zenith angle interval $84^\circ \leq \theta < 90^\circ$). For all other viewing zenith angle intervals the differences are lower than 1%. These differences are within the relative standard errors of the ARF.

We have shown the good agreement between the present Monte Carlo model results for plane-parallel cloud fields and the results reported in independent studies by other authors. The next section concerns radiative quantities of broken cloud fields.

3.1.2. Broken cloud fields. The method used to analyze the radiation field of broken cloud fields is similar to the methods used in overcast conditions. The broken cloud fields are simulated by different cloud fractions or cloud cover c . Only the cloud cell equivalent to the core region contains cloud particles which cause the scattering processes of the radiation.

No other scattering or absorption processes inside or outside the clouds are included in the present model study. Hence the cloud-free wall region surrounding the core region as well as the atmosphere above and below the cloud field are assumed to be completely transparent.

In broken cloud conditions the incoming radiation also illuminates the cloud sides. Mutual shadowing of the clouds is taken into account. The reflected radiation consists of the radiation escaping from the cloud top as well as the upward directed radiation (which does not enter the next cloud) escaping from the cloud sides. The transmitted radiation is enhanced by direct radiation that passes through the cloud-free wall regions (cloud gaps) without interaction processes.

The albedo and the radiation distribution functions described in the previous section are calculated for the radiation field of the broken cloud field and will be discussed here. In the case of broken clouds the radiation entering the cloud gaps illuminates the cloud sides for solar zenith angles $\theta_0 > 0^\circ$ and as a function of the cloud cover c . The albedo and the reflectance/transmittance distribution functions of broken cloud fields are sensitive to the illumination of the cloud sides; that is, the additional in-cloud radiation entering the clouds through the cloud sides contributes to the radiation distribution of the cloud field.

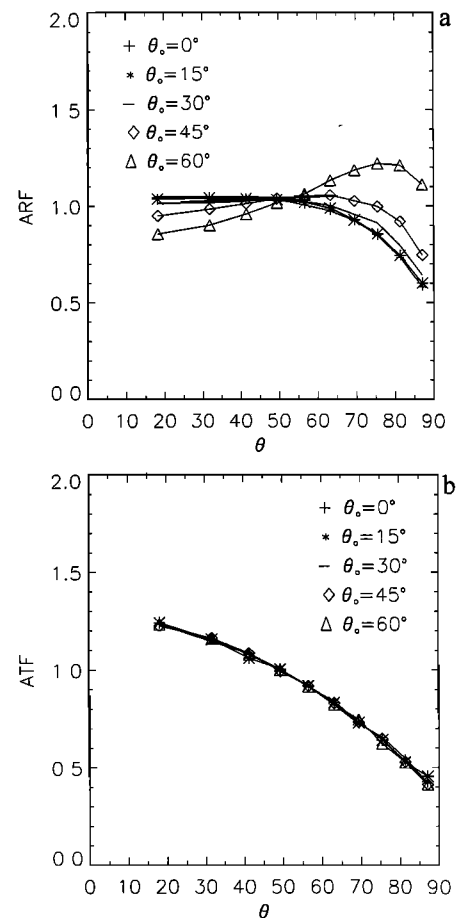


Figure 5. The (a) azimuth-averaged reflectance distribution function (ARF) and (b) the corresponding azimuth-averaged transmittance function (ATF) versus viewing zenith angle θ obtained with the Monte Carlo model for $\tau = 20$ at various solar zenith angles θ_0 .

At low cloud cover the clouds emit a considerable part of the upward and downward escaping radiation through the cloud sides. This so-called side-viewing effect disappears when the neighboring clouds close up.

Table 2 shows the albedo of the cloud field at various degrees of cloudiness and for $\theta_0 = 0^\circ$ and 60° . The optical thickness $\tau = 6, 20,$ and 50 . For $\theta_0 = 0^\circ$ the albedo of broken clouds corresponds well to the fraction c of the albedo in overcast condition, whereas for $\theta_0 = 60^\circ$ the method fails. The nonlinear function of the cloud albedo versus cloud cover c for $\theta_0 = 60^\circ$ demonstrates the influence of the shadowing effect and side-viewing effect in broken cloud fields [Bréon, 1992].

The ARF illustrates the side-viewing effect which decreases with increasing cloud cover c . Figures 7a and 7b depict the ARF at various cloudiness obtained with the Monte Carlo model for ($\tau = 6, \theta_0 = 60^\circ$) and ($\tau = 20, \theta_0 = 0^\circ$), respectively. At cloud cover $c = 30\%$ the side-viewing effect prevails, and the limb darkening is mainly suppressed, in contrast to the cases at $c = 70\%$ and in overcast conditions.

3.1.3. Actinic fluxes. The light available for photodissociation processes is quantified by the actinic flux. In cloudy conditions there are considerable changes in the actinic fluxes; these changes are caused by scattering processes of radiation at cloud particles.

The actinic flux enhancement factor C_F is defined as the ratio between the simulated actinic flux if clouds are present and the clear sky value. In this section we present actinic flux enhancement factors at various degrees of cloudiness.

Table 2. Albedo Obtained With the Monte Carlo Simulation at Various Degrees of Cloudiness for $\tau = 6, 20,$ and 50 and for $\theta_0 = 0^\circ$ and $\theta_0 = 60^\circ$

τ	θ_0	$c = 100\%$	$c = 70\%$	$c = 30\%$
6	0°	28.1%	19.0%	6.6%
	60°	49.9%	42.6%	21.2%
20	0°	61.7%	42.0%	15.0%
	60°	73.8%	63.0%	32.7%
50	0°	81.0%	56.1%	20.5%
	60°	87.1%	75.2%	39.6%

In overcast conditions we simulated actinic flux enhancement factors with the Monte Carlo model for $\tau = 6, 20,$ and 50 and found excellent agreement with the results of the doubling-adding algorithm reported by *van de Hulst* [1980]. The doubling-adding algorithm used in the present study yields the actinic flux enhancement factors versus solar zenith angles for $0.0 < \mu_0 \leq 1.0$ ($\cos \theta_0 = \mu_0$) at cloud top and cloud bottom. The results are shown in Figure 8 for the same parameters as for the Monte Carlo simulation. The asterisks in Figure 8 represent the results of the Monte Carlo simulation for $\theta_0 = 0^\circ, 15^\circ, 30^\circ, 45^\circ,$ and 60° . The simulated actinic flux enhancement factors agree very well with the results of the doubling-adding algorithm and are far below statistical uncertainties.

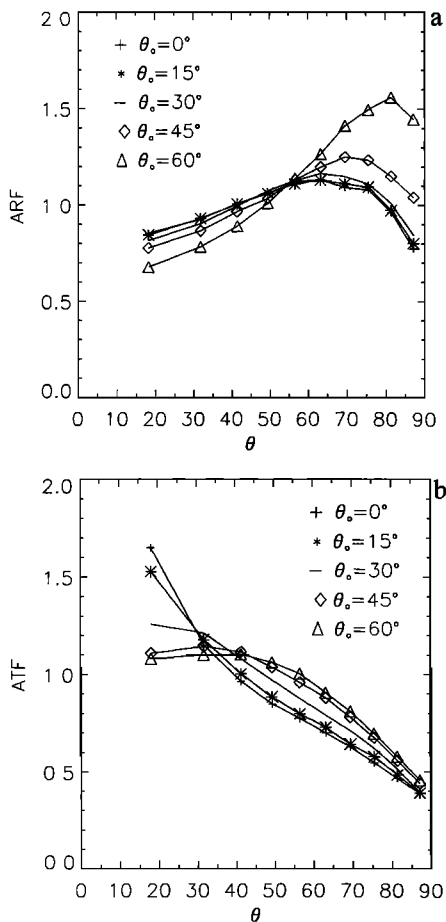


Figure 6. Same as Figure 5, but for $\tau = 6$.

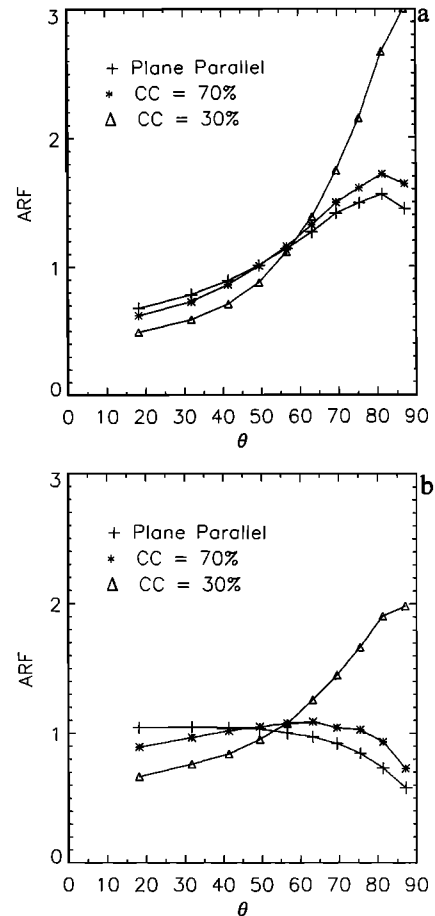


Figure 7. The ARF at various degrees of cloudiness obtained from the Monte Carlo model for (a) $\tau = 6$ and $\theta_0 = 60^\circ$ and for (b) $\tau = 20$ and $\theta_0 = 0^\circ$.

Monte Carlo simulations of in-cloud actinic fluxes in overcast conditions are shown in Figures 9a and 9b for $\theta_0 = 0^\circ$ and 60° , respectively. In Figures 9a and 9b the cloud optical thickness $\tau = 6, 20, \text{ and } 50$. The enhancement of the actinic flux with respect to the clear sky value C_F is plotted on the x axis. The relative cloud height I is plotted on the y axis. As a consequence of the completely transparent atmosphere outside the cloud field, the simulated actinic flux enhancement factors remain constant above and below the cloud field and are equal to the enhancement at the cloud top and cloud bottom, respectively. The main features are the increasing enhancement just below cloud top for $\theta_0 = 0^\circ$, continuously decreasing enhancement with decreasing I for $\theta_0 = 60^\circ$, and the enhancement factor greater than unity below the cloud field for optically thinner clouds with $\tau = 6$.

The scattered radiation increases the photon density in the cloud. This effect causes the peak in the actinic flux enhancement below the cloud top if the incoming radiation is sufficiently diffused, that is, if the Sun is at zenith and the cloud is optically thick ($\tau \geq 20$) (Figure 9a). For $\theta_0 = 60^\circ$, high albedo causes the continuous decrease of the enhancement down through the cloud. Only for optically thin clouds ($\tau \leq 6$) is the albedo at $\theta_0 = 60^\circ$ low enough to permit the photon density just below cloud top to increase so much that the actinic flux enhancement profile reaches its maximum in the cloud (Figure 9b).

With decreasing cloud optical thickness an increasing amount of unscattered, though direct, radiation traverses the clouds. Hence, for optically thin clouds ($\tau \leq 6$) the enhancement factor for $\theta_0 = 0^\circ$ is greater than unity because of the fact that transmitted, unscattered radiation and diffusive radiation increase the photon density over the entire cloud domain (Figure 9a).

The vertical actinic flux profiles of broken cloud fields are shown in Figure 10 for $\tau = 20$ and $\theta_0 = 0^\circ$ at cloud cover $c = 100\%, 70\%, \text{ and } 30\%$. The labels on the axes are the same as in Figure 9a. The mean profiles are plotted with thick lines marked with symbols at each relative cloud height. The corre-

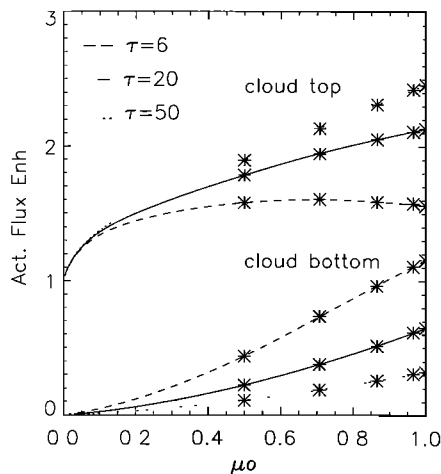


Figure 8. Actinic flux enhancement at cloud top and cloud bottom versus cosine of solar zenith angle, $\mu_0 = \cos(\theta_0)$, obtained with the doubling-adding algorithm for $\tau = 6, 20, \text{ and } 50$. The asterisks indicate the results of the Monte Carlo simulation for the same conditions but for solar zenith angle θ_0 between 0° and 60° in increments of 15° .

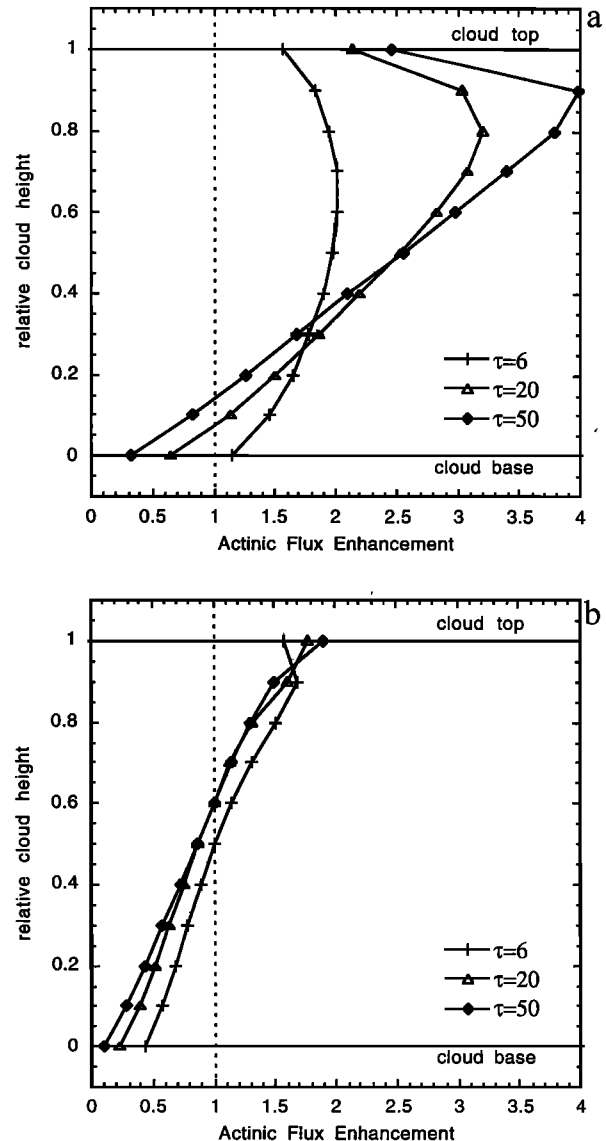


Figure 9. Actinic flux enhancement profiles in overcast conditions obtained with the Monte Carlo simulation for $\tau = 6, 20, \text{ and } 50$ and (a) $\theta_0 = 0^\circ$ and (b) $\theta_0 = 60^\circ$. The horizontal lines at relative cloud heights $I = 1.0$ and 0.0 show the cloud top and cloud bottom, respectively. The dotted line indicates the actinic flux profile if no cloud is present.

sponding maxima and minima of the actinic flux enhancement factors are denoted by the same symbols.

At cloud cover $c = 30\%$ the mean actinic flux enhancement is greater than unity for the whole profile. Enhanced photon density in the cloud gap, due to direct, incoming radiation and diffusive radiation coming from neighboring clouds, increases the overall actinic flux.

By looking at horizontal actinic flux profiles one gains more insight into the highly varying actinic flux enhancement factors. Figures 11a and 11b show the horizontal actinic flux enhancement profiles at cloud cover $c = 70\%$ and 30% , respectively. The profiles are obtained with the Monte Carlo simulation for $\tau = 20$ and $\theta_0 = 0^\circ$ and are presented for the relative cloud heights $I = 1.0, 0.8, \text{ and } 0.0$. The radius R of the hexagonal cell and the hexagonal ring number are plotted on the x axes. The cloud cell region is between the cloud center (hexagonal

ring number 1) and the cloud edge (vertical solid line). The cloud gap extends from the cloud edge to the border of the hexagonal cell (hexagonal ring number 25). The enhancement of the actinic flux C_F is plotted on the y axis.

The horizontal actinic flux enhancement factors in the cloud region decrease continuously toward the cloud edge. Scattered photons are more likely to escape near the cloud edge than far inside the cloud cell. This effect dominates at the relative cloud height $I = 0.8$ where the strongest decrease is found. In the cloud gap region the diffusive radiation coming from the cloud sides is enhanced by direct, incoming radiation. Hence, at $c = 70\%$ and 30% the actinic flux enhancements are greater than unity and depend on the dimensions of the cloud gap. Because of increased photon density the narrow cloud gap (at $c = 70\%$) produces higher enhancement factors than the large cloud gap at $c = 30\%$. For $I = 1.0$ and 0.0 the actinic flux enhancement factors have trends toward constant values which indicate that the photon density in the cloud gap region is the same at cloud top and cloud bottom. For $I = 0.8$ this trend is only found for the large cloud gap (at $c = 30\%$).

The vertical actinic flux enhancement profiles at cloud cover $c = 70\%$ and 30% (Figure 10) depict the mean values of the horizontal actinic flux enhancement factors. Figures 11a and 11b show horizontal actinic flux enhancement profiles at the relative cloud heights $I = 1.0, 0.8,$ and 0.0 . These relative cloud heights are located at the levels that correspond to the extrema of the vertical profiles. The intermediate horizontal profiles are thus enclosed by the given horizontal actinic flux enhancement profiles in Figures 11a and 11b.

4. Summary and Conclusions

For the first time a Monte Carlo simulation method has been used to investigate the effects that cloud fields at various

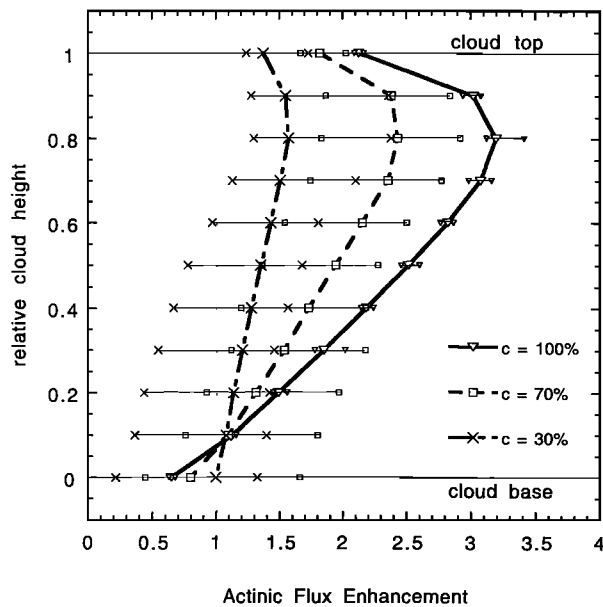


Figure 10. Vertical actinic flux profiles obtained with the Monte Carlo model for $\tau = 20$ and $\theta_0 = 0^\circ$ at various degrees of cloudiness. The maxima and minima are given for each relative cloud height. The horizontal lines at relative cloud heights $I = 1.0$ and 0.0 show the cloud top and cloud bottom, respectively. The dotted line indicates the actinic flux profile if no cloud is present.

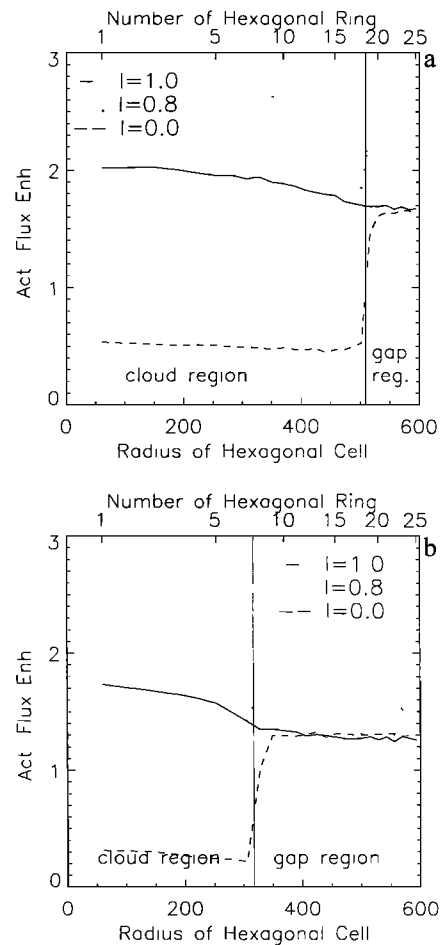


Figure 11. Horizontal actinic flux profiles from cloud center (hexagonal cell number 1) to the edge of hexagonal cell (hexagonal cell number 25) at relative cloud heights $I = 1.0$ (cloud top), 0.8 , and 0.0 (cloud bottom) obtained with the Monte Carlo model for $\tau = 20$ and $\theta_0 = 0^\circ$. Cloud cover $c =$ (a) 70% and (b) 30% . The vertical line limits the inner cloud region.

degrees of cloudiness have on actinic fluxes. The cloud field is composed of hexagonal cells. As such, an infinite domain can be simulated with one single cell. The top and bottom of the cloud field are flat surfaces. Each hexagonal cell contains a hexagonal core region (cloud region) and a cloud free wall region. Only the core regions contain cloud particles (homogeneously distributed) that cause the scattering processes of the radiation. No other scattering or absorption processes are considered in or outside the clouds. Although only one cell is considered, mutual shadowing is taken into account due to periodic boundary conditions. Statistical analysis of the Monte Carlo method revealed that 5×10^5 photons are needed to obtain statistical uncertainties lower than 10% for the simulated radiative quantities.

The simulated actinic flux enhancement factors (relative to the clear sky value) of plane-parallel clouds show excellent agreement with enhancement factors obtained with the doubling-adding algorithm. This agreement, together with the 0.1% accuracy of the doubling-adding algorithm, emphasizes the appropriateness of our actinic flux simulation methods.

Our simulations of the albedo and the radiative distribution functions (ARF and BRDF and the corresponding transmit-

tance functions) are compared with results of earlier studies reported by other authors. In overcast conditions and for broken cloud fields the differences between the model studies are found to be within statistical uncertainties.

A derivation of actinic fluxes from radiative quantities is given (e.g., ARF and albedo for the actinic flux at cloud top). Actinic fluxes are also obtained by the direct simulation method. Differences between the direct method and the calculation of actinic fluxes from radiative quantities are within statistical uncertainties. The direct method also allows horizontal and vertical in-cloud enhancement profiles to be represented at various degrees of cloudiness and for different solar zenith angles and cloud optical depths.

Mean actinic fluxes at cloud top can be up to 3 times higher than the clear sky value. Consequently, photodissociation rate coefficients that depend on the actinic fluxes are changed by the same amount. For broken cloud fields, drastic changes in the actinic flux profiles at cloud edges can be found, whereas the enhancement factors are highest in overcast conditions just below cloud top.

Future model studies on actinic fluxes will have to include absorption and other scattering processes, and model results will have to be compared with observations at various degrees of cloudiness. This should enable us to develop parametrizations of actinic fluxes and photodissociation rate coefficients for different cloud conditions.

Acknowledgments. The Monte Carlo model was developed by P. R. Jonas (Pure and Applied Physics Department, UMIST, United Kingdom) and kindly made available to us.

References

- Barker, H. W., Solar radiative transfer for wind-sheared cumulus cloud fields, *J. Atmos. Sci.*, *51*, 1141–1156, 1994.
- Bréon, F. M., Reflectance of broken cloud fields: Simulation and parametrization, *J. Atmos. Sci.*, *49*, 1221–1232, 1992.
- Coakley, J. A., Reflectivities of uniform and broken layered clouds, *Tellus, Ser. B*, *43*, 420–433, 1991.
- Damiano, P., and P. Chylek, Shortwave radiative properties of clouds: Numerical study, *J. Atmos. Sci.*, *51*, 1223–1233, 1994.
- de Haan, J. F., P. B. Bosma, and J. W. Hovenier, The adding method for multiple scattering computations of polarized light, *Astron. Astrophys.*, *183*, 371–391, 1987.
- Demerjian, K. L., K. L. Schere, and J. T. Peterson, Theoretical estimates of actinic (spherically integrated) flux and photolytic rate constants of atmospheric species in the lower troposphere, *Adv. Environ. Sci. Technol.*, *10*, 369–459, 1980.
- Filyushkin, V. V., and D. K. Lilly, Application of a 3D delta-Eddington radiative transfer model to calculation of solar heating and photolysis rates in a stratocumulus cloud layer, *Proceedings Atmospheric Radiation, Tromsø, Norway, June 30 to July 1, 1993, Proc. SPIE Int. Soc. Opt. Eng.*, *2049*, 56–66, 1993.
- Finlayson-Pitts, B. J., and J. N. Pitts, *Atmospheric Chemistry: Fundamentals and Experimental Techniques*, John Wiley, New York, 1986.
- Hansen, J. E., and L. D. Travis, Light scattering in planetary atmospheres, *Space Sci. Rev.*, *16*, 527–610, 1974.
- Jonas, P. R., Effects of variations of cloud microphysical properties on cloud reflectance, in *Proceedings of 11th International Conference on Clouds and Precipitation, Montreal, August 17–21*, pp. 807–810, Elsevier, New York, 1992.
- Jonas, P. R., On the reflectance of cellular cloud layers, *Q. J. R. Meteorol. Soc.*, *120*, 221–229, 1994.
- Junkermann, W., Measurements of the $J(O^1D)$ actinic flux within and above stratiform clouds and above snow surfaces, *Geophys. Res. Lett.*, *21*, 793–796, 1994.
- Kobayashi, T., Reflected solar flux for horizontally inhomogeneous atmospheres, *J. Atmos. Sci.*, *48*, 2436–2447, 1991.
- Kobayashi, T., Effects due to cloud geometry on biases in the albedo derived from radiance measurements, *J. Clim.*, *6*, 120–128, 1993.
- Lelieveld, J., and P. J. Crutzen, The role of clouds in tropospheric photochemistry, *J. Atmos. Chem.*, *12*, 229–267, 1991.
- Li, J., D. J. W. Geldart, and P. Chylek, Perturbation solution for 3D radiative transfer in a horizontally periodic inhomogeneous cloud field, *J. Atmos. Sci.*, *51*, 2110–2122, 1994a.
- Li, J., D. J. W. Geldart, and P. Chylek, Solar radiative transfer in clouds with vertical internal inhomogeneity, *J. Atmos. Sci.*, *51*, 2542–2552, 1994b.
- Madronich, S., Photodissociation in the atmosphere, 1, Actinic flux and the effects of ground reflections and clouds, *J. Geophys. Res.*, *92*, 9740–9752, 1987.
- Nicholls, S., and J. Leighton, An observational study of the structure of stratiform cloud sheets, I, Structure, *Q. J. R. Meteorol. Soc.*, *112*, 431–460, 1986.
- Pomraning, G. C., On the Henyey-Greenstein approximation to scattering phase functions, *J. Quant. Spectrosc. Radiat. Transfer*, *39*, 109–113, 1988.
- Ruggaber, A., R. Dlugi, and T. Nakajima, Modelling radiation quantities and photolysis frequencies in the troposphere, *J. Atmos. Chem.*, *18*, 171–210, 1994.
- Stammes, P., Influence of clouds on shortwave radiative flux profiles and polarization, in *Proceedings of the International Radiation Symposium: Current Problems in Atmospheric Radiation*, edited by S. Keevallik and O. Kramer, pp. 129–132, A. Deepak, Hampton, Va., 1993.
- Stephens, G. L., Radiative transfer through arbitrarily shaped optical media, II, Group theory and simple closures, *J. Atmos. Sci.*, *45*, 1837–1848, 1988.
- Takano, Y., and K. N. Liou, Radiative transfer in cirrus clouds, III, Light scattering by irregular ice crystals, *J. Atmos. Sci.*, *52*, 818–837, 1995.
- Tsay, S. C., and K. Stammes, Ultraviolet radiation in the Arctic: The impact of potential ozone depletions and cloud effects, *J. Geophys. Res.*, *97*, 7829–7840, 1992.
- van de Hulst, H. C., *Multiple Light Scattering: Tables, Formulas, and Applications*, vol. 2, pp. 473–476, Academic, San Diego, Calif., 1980.
- van Weele, M., and P. G. Duynkerke, Effect of clouds on the photodissociation of NO₂: Observations and modelling, *J. Atmos. Chem.*, *16*, 231–255, 1993.
- van Weele, M., J. Vilà-Guerau de Arellano, and F. Kuik, Combined measurements of UV-A actinic flux, UV-A irradiance and global radiation in relation to photodissociation rates, *Tellus, Ser. B*, *47*, 353–364, 1995.
- Vilà-Guerau de Arellano, J., P. G. Duynkerke, and M. van Weele, Tethered-balloon measurements of actinic flux in a cloud-capped marine boundary layer, *J. Geophys. Res.*, *99*, 3699–3705, 1994.
- Welch, R. M., and B. A. Wielicki, Stratocumulus cloud field reflected fluxes: The effect of cloud shape, *J. Atmos. Sci.*, *41*, 3085–3103, 1984.
- P. G. Duynkerke, A. Los, and M. van Weele, IMAU, Utrecht University, Princetonplein 5, 3584 CC Utrecht, Netherlands. (e-mail: nduinker@fys.ruu.nl; a.los@fys.ruu.nl; weele@fys.ruu.nl)

(Received January 3, 1996; revised September 25, 1996; accepted October 8, 1996.)